THE ASTROPHYSICAL JOURNAL, 543:417–424, 2000 November 1

RESTORATION OF THE *ASCA* SOURCE POSITION ACCURACY

E. V. GOTTHELF[1]
ASCA Guest Observer Facility, NASA/Goddard Space Flight Center, Greenbelt, MD 20771

AND

Y. UEDA, R. FUJIMOTO, T. KII, AND K. YAMAOKA
Institute of Space and Astronautical Science, 3-1-1 Yoshinodai, Sagamahara, Kanagawa 229, Japan; ueda@astro.isas.ac.jp, kii@astro.isas.ac.jp, fujimoto@astro.isas.ac.jp, yamaoka@astro.isas.ac.jp
Received 2000 March 3; accepted 2000 June 15

ABSTRACT

We present a calibration of the absolute pointing accuracy of the *Advanced Satellite for Cosmology and Astrophysics* (*ASCA*) which allows us to compensate for a large error (up to 1′) in the derived source coordinates. We parameterize a temperature dependent deviation of the attitude solution which is responsible for this error. By analyzing *ASCA* coordinates of 100 bright active galactic nuclei, we show that it is possible to reduce the uncertainty in the sky position for any given observation by a factor of 4. The revised 90% error circle radius is then 12″, consistent with preflight specifications, effectively restoring the full *ASCA* pointing accuracy. Herein, we derive an algorithm which compensates for this attitude error and present an internet-based table to be used to correct post facto the coordinate of all *ASCA* observations. While the above error circle is strictly applicable to data taken with the on-board Solid-state Imaging Spectrometers (SISs), similar coordinate corrections are derived for data obtained with the Gas Imaging Spectrometers (GISs), which, however, have additional instrumental uncertainties. The 90% error circle radius for the central 20′ diameter of the GIS is 24″. The large reduction in the error circle area for the two instruments offers the opportunity to greatly enhance the search for X-ray counterparts at other wavelengths. This has important implications for current and future *ASCA* source catalogs and surveys.

Subject headings: instrumentation: miscellaneous — space vehicles: instruments — X-rays: general

1. INTRODUCTION

The broadband spectro-imaging capabilities of the *Advanced Satellite for Astrophysics and Cosmology* (*ASCA*; Tanaka, Inoue, & Holt 1994) has opened up a new parameter space for X-ray astronomy. Spectrally resolved images of the sky in the 0.5–10 keV bandpass have revealed a population of hard ($\gtrsim$2 keV) X-ray sources previously undetected at the softer X-ray energies typically sampled by earlier X-ray imaging missions. To identify these hard X-ray sources, as well as unidentified soft ($\lesssim$2 keV) *ASCA* sources, requires substantial follow-up multiwavelength studies. Crucial to the success of these studies are accurate X-ray coordinates, a prerequisite for narrowing down the field of possible candidates.

Several prominent studies are presently underway (e.g., see Hasinger & White 1998 for an overview). These include, for example, the *ASCA* Large Sky Survey (Ueda et al. 1998; Ueda et al. 1999a; Akiyama et al. 1998; Sakano et al. 1998, the *ASCA* Deep Sky Survey (Ogasaka et al. 1998; Ohta et al. 1998), the *ASCA* Medium Sensitivity Survey (Takahashi et al. 1998; Cagnoni, della Ceca & Maccacaro 1998; della Ceca et al. 1999; Ueda et al. 1999b), the Deep *ROSAT* Fields Survey (Georgantopoulos et al. 1997; Boyle et al. 1998a; Boyle et al. 1998b; Georgantopoulos et al. 1999) and the SIS and GIS source catalogs (Gotthelf & White 1997; Ueda et al. 2000). Furthermore, the search for counterparts to gamma-ray bursts (e.g., Murakami et al. 1994) and unidentified EGRET sources (e.g., Roberts, Romani & Kawai 2000) holds the promise of great scientific breakthroughs.

Follow-up studies for these important projects have been hampered by the *ASCA*'s large (arcminute) error circle, much larger than expected based on preflight specifications. It is clear that any attempt to identify *ASCA* sources is strongly dependent on the accuracy of the derived coordinates. To this end, we have undertaken a comprehensive calibration of the assigned *ASCA* coordinate system with the goal of restoring the pointing accuracy to the preflight expected value of $\sim$10″. To calibrate and illustrate our method, we analyzed a sample of 100 active galactic nuclei (AGNs) observed with *ASCA* for which accurate (arcsec) positions are known. The results presented herein represent a substantial added value toward the overall scientific success of the *ASCA* mission.

In the following, we present our AGN source list and describe our data reduction and analysis method (§ 2), detail a temperature dependent error in the *ASCA* pointing determination (§ 3), and finally, provide a calibration which allows one to significantly improve the *ASCA* derived source sky positions (§ 4). In Table 1 we tabulate the list of AGNs used in this study and give a sample sky offset used to correct the measured *ASCA* coordinates. The full table listing the offset corrections for all *ASCA* observation is available via the internet, along with further documentation and software to apply these corrections (see § 4).

2. OBSERVATIONS

The primary science package on board the *ASCA* observatory consists of four co-aligned X-ray telescopes. Each telescope focuses X-rays using a grazing incident mirror onto one of two types of imagers. In this calibration, we are

[1] Present address: Columbia Astrophysics Laboratory, Columbia University, 550 West 120th Street, New York, NY 10027; evg@astro.columbia.edu

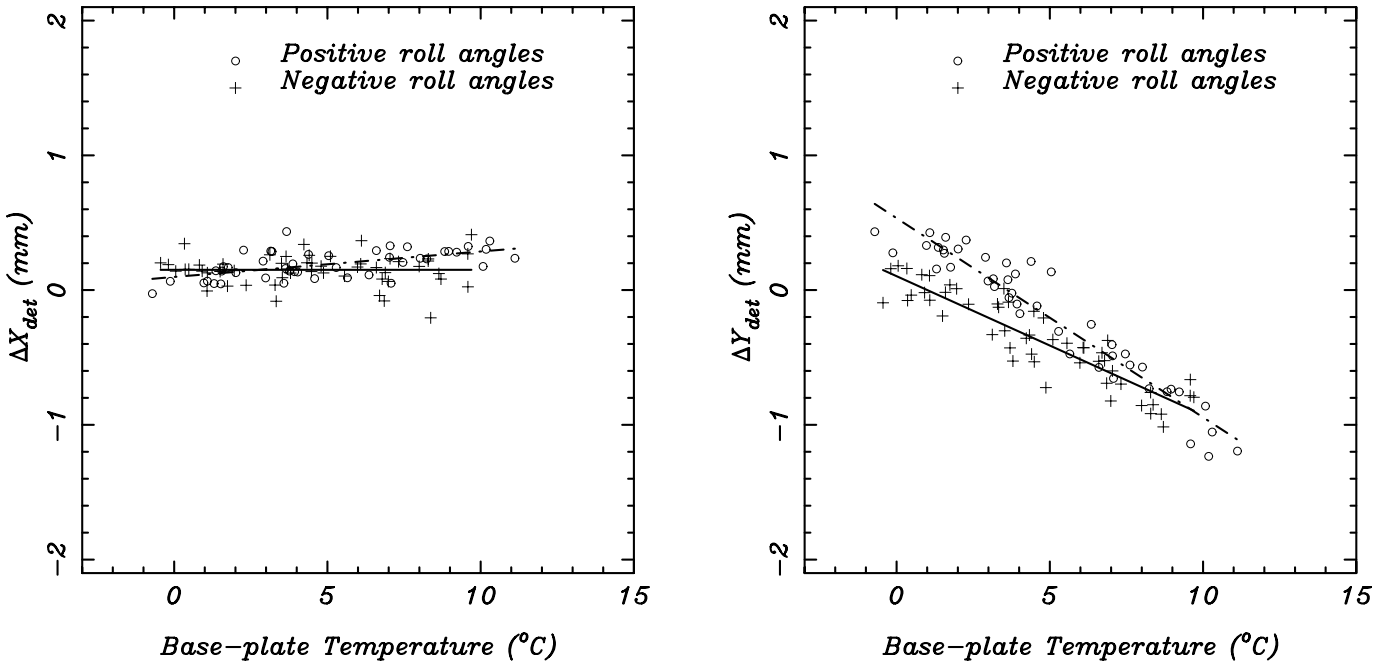

FIG. 1.—Temperature dependence of the *ASCA* SIS detector coordinates. (*Left*) The correlation between the X_{det} (DET-X) offset and the base-plate temperature. (*Right*) The correlation for the Y_{det} (DET-Y) coordinate offsets, plotted on the same scale. The lines represent the best-fit model to a linear fit depending on the side of the satellite preferentially illuminated by the Sun (see text).

primarily concerned with images created using the two Solid-state Imaging Spectrometers (SISs). Pixel locations of photons read out from these X-ray CCD cameras provide an accurate position fixed in the satellite coordinate plane. Each camera is composed of a square mosaic of four adjacent CCDs, each $11' \times 11'$ on a side, comprising the full SIS field of view (FOV). Sky images formed on the SIS are greatly oversampled by the arcmin point-response function (PSF) of the *ASCA* mirrors with no added image distortion. Although the azimuthally average PSF is characterized by a core of FWHM $\sim 50''$ (Jalota, Gotthelf, & Zoonematkermani 1993), it is possible to measure the positions of moderately bright (~ 1 counts s^{-1}) SIS pointlike sources with a precision of up to $5''$ (see Gotthelf & Ishibashi 1997).

We also calibrate the two Gas Imaging Spectrometers (GISs) which have a similar energy bandpass ($\sim$1–10 keV)

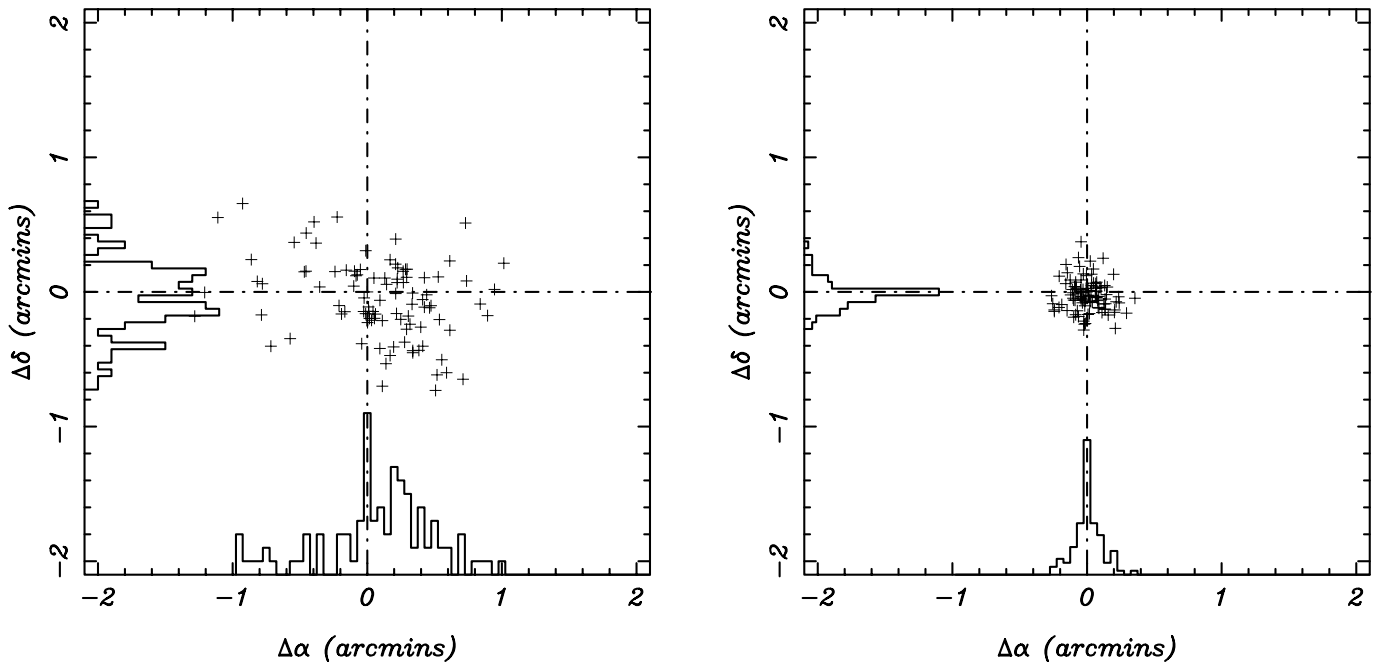

FIG. 2.—(*Left*) Scatter plot of offsets of *ASCA* SIS positions from standard sky coordinates. (*Right*) The same plot obtained after applying the attitude correction described in the text. The histogram of the data projected along the two coordinates illustrates that the error circle for the corrected data is reduced by a factor of 4.

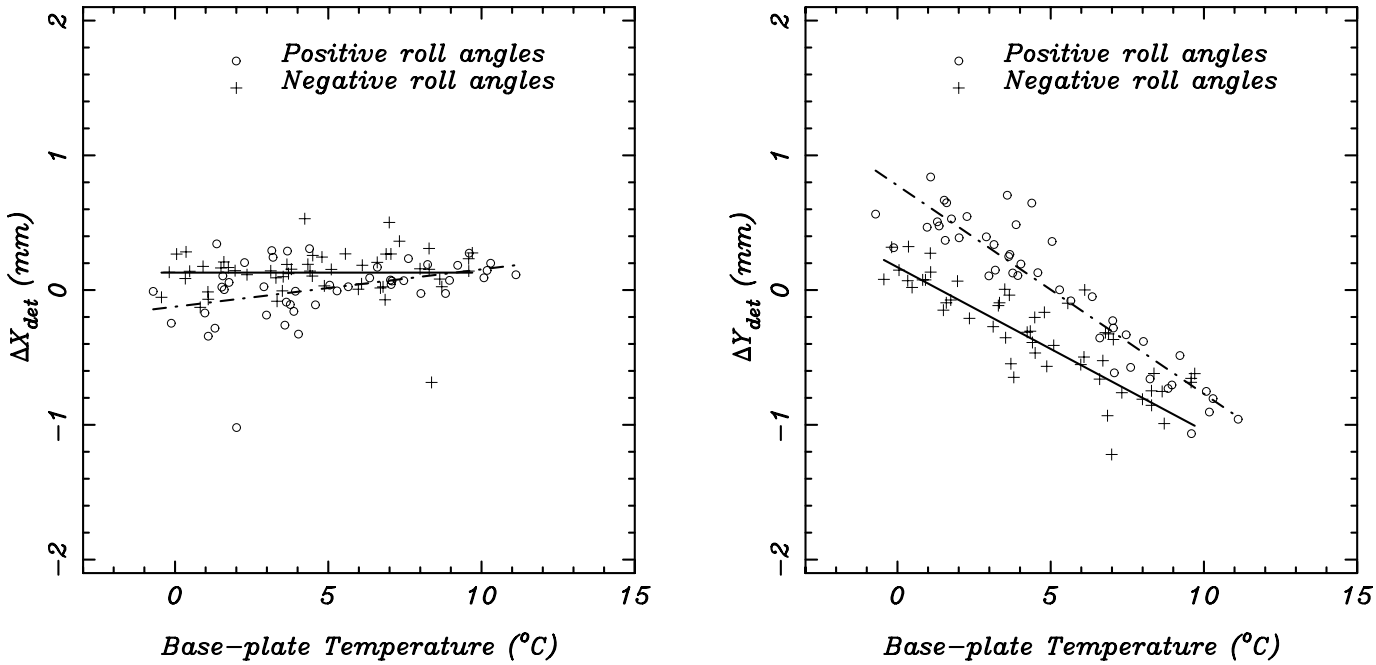

FIG. 3.—Temperature dependence of the *ASCA* GIS detector coordinates. (*Left*) The correlation between the GIS X_{det} (DET-X) offset and the base-plate temperature. (*Right*) The correlation for the GIS Y_{det} (DET-Y) coordinate offsets. Lines and scaling same as for Fig 2.

but larger FOV ($\sim 30'$). However, its instrumental blur, window support structure, and temperature dependence, all conspire to introduce additional uncertainties in their measured source positions (see § 4 for a discussion).

The main data set used in this study is a collection of AGNs and quasars from the 8th Edition of the Veron catalog (Veron-Cetty & Veron 1998) which have precise (arcsec) celestial coordinates. We selected about 100 cataloged objects which were detected by the SIS as pointlike sources with a significance $> 10\,\sigma$, but were not so bright as to saturate the CCD pixels, which could produce additional uncertainties in the measured coordinate. Our final source list is given in Table 1, which reproduces the standard coordinates for each AGN and the associated *ASCA* data sets used in this analysis. These observations were acquired over the course of the mission, up to the end of 1996, using one of three possible SIS CCD configurations (1-, 2-, or 4-CCD mode). It should be noted that this list represents a subset of

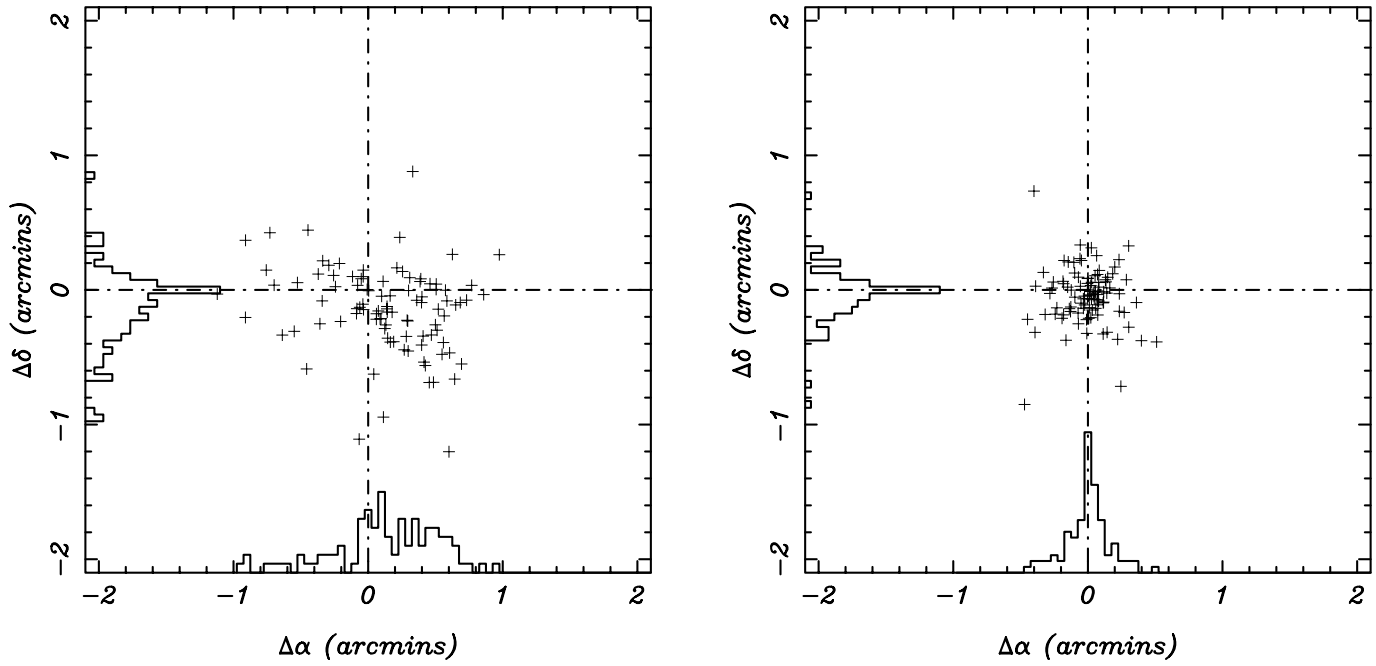

FIG. 4.—(*Left*) Scatter plot of offsets of *ASCA* GIS positions from standard sky coordinates. (*Right*) The same plot obtained after applying the attitude correction described in the text. The histogram of the data projected along the two coordinates illustrates that the central core of the error circle for the corrected data set is similar to that found with the SIS.

TABLE 1

STANDARD COORDINATES OF REFERENCE ACTIVE GALACTIC NUCLEI USED IN THIS STUDY

Object[a]	Right Ascension (FK5 J2000)	Declination (FK5 J2000)	*ASCA* Sequence Number	*ASCA* Attitude File[b] Observation Date
MRK 937	00 10 10.10	−04 42 38.1	73038000	fa941211_1156.1827
ESO 540−G01	00 34 13.50	−21 26 29.8	73062000	fa951211_0932.1420
MRK 348	00 48 47.20	+31 57 24.4	73072000	fa950804_0805.1240
I ZW 1	00 53 34.88	+12 41 35.7	73042000	fa950715_1200.1400
PHL 909	00 57 09.88	+14 46 10.7	74077000	fa960118_0257.1540
NGC 315	00 57 48.88	+30 21 08.6	74000000	fa960805_1643.1641
PKS 0208−512	02 10 46.27	−51 01 01.2	73086000	fa950115_2044.0540
MRK 1040	02 28 14.37	+31 18 40.6	72016000	fa940819_1644.0520
NGC 985	02 34 37.77	−08 47 14.8	74053000	fa960812_0846.1315
AO 0235+16	02 38 38.89	+16 36 59.1	71015000	fa940204_1907.0441
NGC 1052	02 41 04.76	−08 15 20.7	74061000	fa960811_0216.0846
2E 0323+0214	03 26 13.85	+02 25 14.1	71034000	fa940124_0326.0635
NRAO 140	03 36 30.05	+32 18 29.4	71047000	fa940201_2356.0140
2E 0414+0057	04 16 52.34	+01 05 23.9	74093000	fa960830_0617.0537
PKS 0528+134	05 30 56.42	+13 31 54.6	72030000	fa940828_1420.0140
PKS 0528+134	05 30 56.42	+13 31 54.6	73054010	fa950307_0522.2250
MCG−8−11−11	05 54 53.51	+46 26 20.5	73052000	fa950903_0515.1310
MRK 3	06 15 36.23	+71 02 14.0	74041000	fa961026_0729.0401
PKS 0634−20	06 36 32.12	−20 34 52.7	73058000	fa951009_0756.1530
S4 0636+68	06 42 03.92	+67 58 35.2	74003000	fa961024_1520.2301
S5 0716+71	07 21 53.21	+71 20 34.9	71006000	fa940316_1945.0620
PKS 0735+17	07 38 07.29	+17 42 18.8	74005000	fa960422_2301.2320
4C 55.16	08 34 54.77	+55 34 20.2	74036000	fa961101_0333.0150
S5 0836+71	08 41 24.29	+70 53 41.0	72002010	fa950317_0312.1420
OJ 287	08 54 48.67	+20 06 29.6	15035000	fa941118_1007.1500
3C 215.0	09 06 31.68	+16 46 11.7	83041000	fa951104_1947.1921
IRAS 09104+4109	09 13 45.38	+40 56 26.3	71002000	fa931112_2030.2201
3C 234.0	10 01 49.38	+28 47 09.5	71043000	fa940504_0721.2000
NGC 3147	10 16 53.46	+73 24 01.9	60040000	fa930929_1258.0500
NGC 3227	10 23 30.46	+19 51 55.9	73068000	fa950515_0052.0041
B2 1028+313	10 30 58.98	+31 02 55.6	83063000	fa950503_1913.0540
1ES 1028+511	10 31 18.37	+50 53 35.1	73013000	fa950428_1433.0420
HE 1029−1401	10 31 54.27	−14 16 51.7	73050000	fa951208_2137.0320
KUG 1031+398	10 34 38.46	+39 38 28.5	72020000	fa941119_1504.1630
NGC 3310	10 38 45.75	+53 30 11.1	61013000	fa940417_0904.2031
4C 06.41	10 41 17.07	+06 10 15.8	74007000	fa961213_0914.1821
3C 249.1	11 04 13.66	+76 58 57.0	74050000	fa961203_1140.0930
3C 254.0	11 14 38.44	+40 37 19.3	74035000	fa961207_1320.1050
PG 1114+445	11 17 06.16	+44 13 33.3	74072000	fa960505_2354.2345
PG 1116+215	11 19 08.66	+21 19 17.8	73064000	fa950519_0904.2102
PG 1148+549	11 51 20.34	+54 37 32.1	73037000	fa951207_2209.2050
NGC 3998	11 57 55.93	+55 27 12.2	71048000	fa940510_1945.1140
PG 1211+143	12 14 17.52	+14 03 12.7	70025000	fa930603_1236.0235
WAS 49b	12 14 17.65	+29 31 42.9	73036000	fa950522_2007.2130
MRK 766	12 18 26.55	+29 48 46.7	71046000	fa931218_0221.0040
NGC 4258	12 18 57.34	+47 18 13.4	64001000	fa960523_0645.0350
PG 1216+069	12 19 20.74	+06 38 37.9	74074000	fa951225_1012.2250
NGC 4450	12 28 29.33	+17 05 06.8	63013000	fa950620_0504.0951
PG 1244+026	12 46 35.13	+02 22 08.0	74070000	fa960701_2204.0430
PG 1247+267	12 50 05.54	+26 31 06.6	73048000	fa950617_1221.1621
NGC 4736	12 50 53.04	+41 07 17.5	63020000	fa950525_1726.1940
3C 279	12 56 11.17	−05 47 21.5	70026000	fa930621_2208.1754
MRK 231	12 56 14.04	+56 52 24.2	72044000	fa941205_0444.1850
B2 1308+32	13 10 28.53	+32 20 43.7	74094000	fa960610_1516.0200
NGC 5005	13 10 56.13	+37 03 31.5	73027000	fa951213_0737.0800
NGC 5033	13 13 27.33	+36 35 37.5	63012000	fa951214_0801.0800
NGC 5135	13 25 43.82	−29 50 01.6	73071000	fa950122_1654.1820
IRAS 13349+2438	13 37 18.61	+24 23 03.5	73056000	fa950627_1454.2230
VV98c J134009.3+271838	13 40 09.11	+27 18 37.8	73020000	fa950703_1304.2210
RXS J13410+3959	13 41 04.81	+39 59 44.3	83049000	fa950627_2233.2128
RX J13434+0001	13 43 29.03	+00 01 32.8	74047000	fa960112_0753.0600
MRK 273	13 44 41.91	+55 53 12.1	73014000	fa941227_1919.1941
PG 1404+226	14 06 21.71	+22 23 46.7	72021000	fa940713_0245.0641
PG 1411+442	14 13 48.10	+44 00 13.4	74075000	fa961208_1055.1230

TABLE 1—*Continued*

Object[a]	Right Ascension (FK5 J2000)	Declination (FK5 J2000)	*ASCA* Sequence Number	*ASCA* Attitude File[b] Observation Date
PG 1416−129	14 19 03.60	−13 10 44.9	72043000	fa940729_2222.2021
B 1422+231	14 24 37.90	+22 56 00.6	73078000	fa950114_0909.0910
B2 1425+26	14 27 35.52	+26 32 13.5	74073000	fa960726_0311.0440
H 1426+428	14 28 32.50	+42 40 20.4	71044000	fa940206_0229.1730
MRK 477	14 40 37.90	+53 30 15.1	73028000	fa951204_0637.2220
PG 1440+356	14 42 07.29	+35 26 22.4	73067000	fa950702_1254.1301
3C 303	14 43 02.57	+52 01 36.5	73008000	fa950521_1745.2003
MRK 841	15 04 01.00	+10 26 15.9	70009000	fa930822_0212.0205
GB 1508+5714	15 10 02.61	+57 02 46.2	73080000	fa950302_1536.1340
PKS 1510−08	15 12 50.30	−09 05 59.8	74082000	fa960820_1248.0640
MRK 290	15 35 52.09	+57 54 08.2	72027000	fa940615_1158.1631
KAZ 49	15 57 03.08	+63 50 27.1	63015000	fa950213_2250.1101
2E 1615+0611	16 17 45.30	+06 03 55.0	73051000	fa950820_1221.0803
NGC 6251	16 32 31.78	+82 32 14.9	72035000	fa941028_1658.1530
PG 1634+706	16 34 28.77	+70 31 31.9	71036000	fa940502_1959.1331
3C 346.0	16 43 48.38	+17 15 47.6	73092000	fa950217_1925.1430
B3 1702+457	17 03 30.47	+45 40 44.5	73047000	fa950829_1332.1317
PG 1718+481	17 19 38.17	+48 04 12.4	71037000	fa940501_1822.1200
OT 081	17 51 32.57	+09 39 02.0	73087000	fa950922_1034.0915
3C 371.0	18 06 50.48	+69 49 26.9	74086000	fa961105_1126.1531
3C 390.3	18 42 08.76	+79 46 16.0	71008000	fa931116_2203.2330
3C 411.0	20 22 08.13	+10 01 11.8	72018000	fa941023_0304.1851
4C 74.26	20 42 37.02	+75 08 01.0	74097000	fa960909_1452.0300
IRAS 20460+1925	20 48 17.63	+19 36 56.6	72015000	fa941027_0607.0741
RX J2144.5+1446	21 44 30.91	+14 46 43.8	23044010	fa951110_2236.1221
NGC 7172	22 02 01.60	−31 52 07.6	73057000	fa950512_2318.1600
BL LAC	22 02 43.00	+42 16 38.4	73088000	fa951122_0103.1951
NGC 7314	22 35 45.81	−26 03 01.8	74059000	fa960518_0652.0820
NGC 7319	22 36 03.20	+33 58 32.4	62002000	fa941207_1357.1820
PKS 2236−047	22 39 32.54	−04 29 33.6	83018000	fa950531_0647.1052
MR 2251−178	22 54 05.60	−17 34 54.6	74028000	fa960526_0018.1600
IRAS 23060+0505	23 08 33.71	+05 21 29.8	74012000	fa960614_1335.1835
ZW 478.002	23 55 47.88	+25 30 31.7	74101010	fa961222_1622.1441

NOTE.—Units of right ascension are hours, minutes, and seconds, and units of declination are degrees, arcminutes, and arcseconds.

[a] Names as given in the Veron catalog (Veron-Cetty & Veron 1998) when available, otherwise the preferred X-ray name is used.

[b] Attitude file name with the observation date encoded "faYYMMDD_HHMM.HHMM", where YYMMDD gives the observation year/month/day and HHMM represents the start and stop time in hours/minutes

ASCA AGNs, as many others fell outside the SIS FOV, but were still seen by the GIS, with its larger FOV (cf. the TAUTARUS *ASCA* AGN database, Turner et al. 2000).

The data sets for each AGN were obtained from the public archive and have been processed with the latest revision of the pipeline software. We extracted images and exposure maps using the standard analysis tools available from the data center. These results were double checked using local software. For each contiguous observation, a single merged and exposure-corrected image was produced by co-adding data sets of each instrument type (SIS or GIS). The SIS images were rebinned by a factor of 4 (320 × 320 pixel images); we used only those GIS observations acquired in default spatial mode (256 × 256 pixel images).

TABLE 2

SAMPLE CORRECTION VALUES FOR THE *ASCA* IMAGE COORDINATES

ASCA Sequence Number	*ASCA* Attitude File[a] Observation Date	SIS[b]		GIS[b]	
		Δα (arcmin)	Δδ (arcmin)	Δα (arcmin)	Δδ (arcmin)
70025000	fa930603_1236.0235	0.159862	−0.165195	0.073714	−0.185680
...	...	...	...	...	...

[a] Attitude file name with the observation date encoded "faYYMMDD_HHMM.HHMM", where YYMMDD gives the observation year/month/day and HHMM represents the start and stop time in hours/minutes.

[b] For images using data merged from both instruments pairs (SIS0 + SIS1 or GIS2 + GIS3).

These images form the basis for measuring the *ASCA* source positions used herein.

3. THE *ASCA* POINTING: PROBLEM AND RESOLUTION

The celestial coordinates of astronomical sources measured by *ASCA* are determined using the attitude solution which gives the satellite bore sight as a function of time. Ultimately, the absolute pointing of the satellite is derived from (optical) guide stars, whose locations are accurately known to $\lesssim 1''$, imaged by a pair of on-board star trackers. Signals from these star trackers are used for real-time guiding and to track the satellite aspect, allowing post facto reconstruction of the instantaneous pointing. During maneuvers or when guide stars are otherwise unavailable (i.e., Earth block or South Atlantic Anomaly), the relative satellite aspect is determined by a set of on-board gyroscopes. During the nominal pointed observations the absolute attitude is updated using the star-tracker data.

Initial in-orbit calibration of *ASCA* 's attitude control system revealed a $\sim 1'$ orbital modulation between the relative gyroscope and star tracker solutions (Ninomiya et al. 1994). The reason for this anomalous behavior was not well understood at the time but thought to be related to the star tracker signal and to thermal cycling of the spacecraft during its orbit (Kii 1993). As a remedy, the guiding function of the star trackers was effectively suppressed.

Since then, a comprehensive postlaunch, end-to-end calibration of *ASCA*'s attitude solution (Gotthelf 1996) confirmed that the spacecraft pointing is stable during targeted observations, with an intrinsic rms of 0.2. However, a larger than expected ($\sim 1'$) uncertainty was found in the derived coordinates, producing a 40″ radius error circle at the 90% confidence level. This additional uncertainty is found to result from a systematic offset in the absolute X-ray coordinate of the sky image produced for a given observation. It was thus reasoned that a simple relationship might be found to correct this problem.

An investigation by Ueda et al. (1999b) has subsequently isolated the cause of the attitude problem to a temperature dependent alignment variation of the star trackers relative to the science instruments. The apparent position of a guide star wanders up to 1′ and thus generates a false reading for the X-ray pointing. Here we present a refined relationship between the apparent mispointing, the satellite solar illumination geometry, and the temperature of the base-plate on which the star-tracker sits. This is used to compute corrections, which effectively restores the nominal operation of the attitude control system.

4. WELL-TEMPERED *ASCA* COORDINATES

In order to calibrate the sky image offsets we used the sample of AGNs presented in Table 1. For each source, we computed the difference between the true (known) celestial coordinate (α_o, δ_o) and that measured by the *ASCA* SIS camera (α, δ) and examined the collective scatter of these offsets which we refer to as ($\Delta\alpha$, $\Delta\delta$). Source detection was done using a fairly simple method to ensure a robust and model independent result. First, we located the X-ray peak in the flat-fielded images which lies within 2′ of the expected source. Next, we determined a refined position using a centroid calculation for the first moments in α and δ. Finally, following the method outlined in Ueda et al. (1999b), we plotted the offsets, rotated into the detector coordinate system, $\Delta X_{\rm det}$, $\Delta Y_{\rm det}$[2], against $\langle T_{\rm bp}\rangle$, the base-plate temperature, averaged over each observation during periods when the star-tracker derived attitude solution was available (~ 20 minutes per orbit). These results are plotted in Figure 1.

We further considered the effect of roll angle on the scatter and found that a significant reduction can be achieved by considering the Solar illuminated geometry of the satellite as parameterized by the satellite roll angle. In Figure 1 we have plotted separately data from two roll angle domains, which we refer to as positive roll angle (roll angle $\theta > 180^\circ$ or simply θ^+) and negative roll angle ($\theta < 180^\circ$ or θ^-). For both roll angle regimes, we find a strong correlation between the $Y_{\rm det}$ offsets and the averaged base-plate temperature, and to a lesser extent with the $X_{\rm det}$ offsets. A linear least-square fit to these data, allowing for the two roll angle domains, yields, for the SIS:

$$\Delta X^{\theta^+}_{\rm det}(') = -0.8675 + 0.0105 \times \langle T_{\rm bp}\rangle \quad (1)$$

$$\Delta Y^{\theta^+}_{\rm det}(') = +8.0969 - 0.0821 \times \langle T_{\rm bp}\rangle \quad (2)$$

$$\Delta X^{\theta^+}_{\rm det}(') = +0.1534 \quad (3)$$

$$\Delta Y^{\theta^+}_{\rm det}(') = +5.3669 - 0.0572 \times \langle T_{\rm bp}\rangle\ . \quad (4)$$

These algorithms give the offset in detector coordinates (in arcmin) for a given observation. Here, $\langle T_{\rm bp}\rangle$ is the averaged base-plate temperature "BP4", in engineering units[3] generally available in the common housekeeping (CMHK) files produced in the standard processing. The constant coefficient for these fits, most evident in the $X_{\rm det}$ coordinate, is likely due to a slight miscalibration in the alignment matrix resulting from the temperature dependence itself in the calibration observation.

We can now determine the correction offsets to the celestial coordinates ($\Delta\alpha$, $\Delta\delta$), in arcmin, from the above detector offsets (eqs. [1]–[4]) using a simple rotation:

$$\Delta\alpha = (-\Delta X_{\rm det}\cos\theta - \Delta Y_{\rm det}\sin\theta)/\cos\delta \quad (5)$$

$$\Delta\delta = (-\Delta X_{\rm det}\sin\theta + \Delta Y_{\rm det}\cos\theta)\ , \quad (6)$$

where θ is again the average roll angle for the pointed observation, available in the *ASCA* event file headers.

The above formula (eqs. [5] and [6]) allows us to correct the coordinates for any given *ASCA* observation in the following sense:

$$\alpha_{\rm corrected} = \alpha_{\rm measured} + \Delta\alpha/60 \quad (7)$$

$$\delta_{\rm corrected} = \delta_{\rm measured} + \Delta\delta/60\ , \quad (8)$$

where α, δ are the coordinates in decimal degrees, and the offsets are in arcminutes. In particular, we can apply these to our SIS source sample and plot the result (Fig. 2) alongside the uncorrected offsets. The position accuracy is evidently greatly improved, with an error radius of 12″ (90%

[2] The detector coordinates, which are referred to in the *ASCA* data files as DET-X/Y, are related to the satellite coordinates ($X_{\rm sat}$, $Y_{\rm sat}$) by $X_{\rm det} = -X_{\rm sat}$ & $Y_{\rm det} = Y_{\rm sat}$, effectively transforming from a "look-down" to a "look-up" perspective.

[3] The base-plate temperature conversion factor from engineering units to degrees centigrade is given by $T(C^\circ) = -50.2 + 0.5459 \times T(BP4)$

confidence), a factor of 4 smaller then previously reported (cf. Figs. 2*a* and 2*b*).

This result is most fortuitous, as we now have a simple prescription by which to correct *all previously measured ASCA source coordinates* without the burden of reprocessing and reanalyzing the data again. Since the offsets are fixed for a given *ASCA* observation, they need only be computed once using the above algorithm for all available data sets. This has been done, and we provide the full list in a Web page dedicated to updating the *ASCA* coordinates which can be found at the following URL: http://legacy.gsfc.nasa.gov/docs/asca/coord/update.html. This site, maintained by the authors in conjunction with the *ASCA* Guest Observed Facility at NASA's Goddard Space Flight Center, contains the latest machine-readable version of the look-up table, along with relevant software and additional documentation.

At this juncture it might be interesting to address the question of why the mean temperature $\langle T_{\rm bp} \rangle$ is sufficient to correct the coordinates, when the temperature can vary significantly over the course of the observation? The answer relies on the fact that the focal plane pointing is not actually changing as a function of time, but the apparent locations of guide stars imaged by the star-trackers are. While the instantaneous coordinate solution reported by the STT wanders (because of temperature dependence) over the focal plane during the portion of the orbit when available, it is the coordinate solution averaged over the observation which is used to determine the absolute coordinate. This introduces an apparent offset in the coordinate which depends on the average base-plate temperature during this period. Thus the average STT signal is well correlated with the average base-plate temperature, allowing us to determine the relationship between the two and correct *ASCA*'s absolute pointing. Furthermore, it should be noted that since the time history of the STT data is not used either for guiding or for instantaneous attitude reconstruction, the X-ray images as seen by the detectors do not manifest any unexpected added attitude related blurring, as the pointing is apparently stable to 0.2′ (i.e., no arcminute wandering is seen in the X-ray images in either the detector or celestial coordinate system).

4.1. *Application to Locating GIS Sources*

We also calibrated the source coordinate positions for the GIS by applying the same prescription as described above. As for the SIS, we measured the GIS position offsets using the AGN sample presented in Table 1 and plotted the GIS offsets versus temperature (Fig. 3). Again, we considered separately the two roll angle domains and obtained the following least-squares fits to a linear model:

$$\Delta X^{\theta+}_{\rm det}(') = -1.5420 + 0.0154 \times \langle T_{\rm bp} \rangle \quad (9)$$

$$\Delta Y^{\theta+}_{\rm det}(') = +8.6943 - 0.0859 \times \langle T_{\rm bp} \rangle \quad (10)$$

$$\Delta X^{\theta+}_{\rm det}(') = +0.1323 \quad (11)$$

$$\Delta Y^{\theta+}_{\rm det}(') = +5.4640 - 0.0578 \times \langle T_{bp} \rangle . \quad (12)$$

The linear coefficients for the above fits are nearly the same as those found for the SIS, within measurement error, as would be expected if the offsets were related only to an error in the star-tracker signal. However, it is somewhat surprising that the fits for the two detector systems differ by a shift as large as ~0.′2; a close inspection of the respective offset plots for the SIS and GIS data shows that this difference is confined to the positive roll angle data *only*. The reason for this is yet unclear.

The error circle which results by applying the above corrections to the measured GIS coordinates is shown in Figure 4. The distribution of offsets is similar to that found for the SIS, but with a few noisy outliers reflecting the increased uncertainty in derived coordinates related to the GIS position measurements and not to any attitude solution error. The 90% error circle for GIS measured sources which fall on the central 20′ diameter of the detector, i.e., for the region which overlaps the SIS area, is 24″. Away from the center of the detector, the GIS error circle for off-axis sources can grow significantly larger due to instrumental effects and measurement limitation. For example, although most of the nonlinear "pincushion" distortion of the spatial coordinates has been removed, the accuracy in the GIS detector coordinates decreases greatly toward the edge of the detector.

Similarly, as the mirror off-axis PSF is asymmetric, measurements of an off-axis source peak will be slightly skewed, once convolved with the GIS response, introducing further uncertainties in the GIS derived coordinates. Outside the central 20′ region of the detector, a conservative estimate suggests an additional 0.′5 uncertainty in the derived GIS coordinate positions increasing to 1′ toward the edge of the detector. Finally, for faint sources there can be a systematic error caused by source confusion. This error can be as large as 0.′6 for a source detected with a significance of less than 10 σ (Ueda et al. 2000).

We note in passing that coordinates derived from GIS data acquired in reduced spatial resolution mode (e.g., 64 × 64 pixels) should be assigned an added 1′ uncertainty, as the small number of GIS observations in this mode are not well calibrated. For completeness, however, we also include the GIS correction offsets for these observations in the look-up table.

5. SUMMARY

We have presented a calibration of *ASCA*'s celestial coordinates that allows us to restore the pointing accuracy. We have found a clear correlation between the offset of the celestial coordinates with temperature and Solar illumination geometry. We have tabulated a set of correction values, available via the internet, which can be applied to any given *ASCA* observation. This correction allows one to improve the *ASCA* derived coordinates of previously measured *ASCA* sources by a factor of 4. The absolute pointing accuracy resulting from this calibration, derived using a set of AGNs from the Veron catalog, is 12″ in radius (90% confidence level). The corrections are most useful for follow-up multiwavelength surveys and catalogs and for understanding similar errors in future space-based satellite observatories.

We thank the NEC ACS team for useful discussion and comments and Jules Halpern for a careful reading of the manuscript. E. V. G. acknowledges the support of NASA LTSA grant NAG5–7935. This research has made use of data obtained through the High Energy Astrophysics Science Archive Research Center On-line Service, provided by the NASA/Goddard Space Flight Center.

REFERENCES

Akiyama, M., et al. 1998, ApJ, 500, 173
Boyle, B. J., Almaini, O., Georgantopoulos, I., Blair, A. J., Stewart, G. C., Griffiths, R. E., Shanks, T. & Gunn, K. F. 1998a, MNRAS, 297, L53
Boyle, B. J., Georgantopoulos, I., Blair, A. J., Stewart, G. C., Griffiths, R. E., Shanks, T., Gunn, K. F. & Almaini, O. 1998b, MNRAS, 296, 1
Cagnoni, I., della Ceca, R. & Maccacaro, T. 1998, ApJ, 493, 54
della Ceca, R. , Castelli, G. , Braito, V. , Cagnoni, I. & Maccacaro, T. 1999, ApJ, 524, 674
Georgantopoulos, I., Stewart, G. C., Blair, A. J., Shanks, T., Griffiths, R. E., Boyle, B. J., Almaini, O., & Roche, N. 1997, MNRAS, 291, 203
Georgantopoulos, I., Almaini, O., Shanks, T., Stewart, G. C., Griffiths, R. E., Boyle, B. J. & Gunn, K. F. 1999, MNRAS, 305, 125
Gotthelf, E. V. 1996, *ASCA* News, 4, 31
Gotthelf, E. V. & Ishibashi, K. 1997, in X-Ray Imaging and Spectroscopy of Cosmic Hot Plasmas, ed. F. Makino & K. Mitsuda (Tokyo: Waseda Univ.), 631
Gotthelf, E. V. & White, N. E. 1997, in X-Ray Imaging and Spectroscopy of Cosmic Hot Plasmas, ed. F. Makino & K. Mitsuda (Tokyo: Waseda Univ.), 31
Hasinger, G. & White, N. E. 1998, Astron. Nachr., 319, 1
Jalota, L., Gotthelf, E. V. & Zoonematkermani, S. 1993, Proc. SPIE, 1945, 453.
Kii, T. 1993, ISAS memo, unpublished.
Murakami, T., Tanaka, Y., Kulkarni, S. R., Ogasaka, Y., Sonobe, T., Ogawara, Y., Aoki, T., Yoshida, A. 1994, Nature, 368, 127
Ninomiya, K., Hasimoto, T., Kii, T., Muranaka, N, Uo, M., Maeda, K., Saitoh, T. 1994, in Advances in the Astronautical Sciences, ed. D. Culp & R. Rausch (San Diego: Univelt Corp.), Guidance and Control (Amer. Astronautical Society), 86, 555
Ogasaka, Y., et al. 1998, Astron. Nachr., 319, 43
Ohta, K., Yamada, T., Akiyama, M., Nakanishi, K., Hayashida, K., Kii, T. & Ogasaka, Y. 1998, Astron. Nachr., 319, 71
Roberts, M. S. E., Romani, R. W., & Kawai, N. 2000, ApJ, submitted
Sakano, M., et al. 1998, ApJ, 505, 129
Takahashi, T., Ueda, Y., Ishisaki, Y., Ohashi, T. & Makishima, K. 1998, Astron. Nachr., 319, 91
Tanaka, Y., Inoue, H. & Holt, S. S. 1994, PASJ, 46(3), L37
Turner, T. J., Nandra, K., Turcan, D., & George, I. M. 2000, Astrophys. Lett. Commun., in press
Ueda, Y., et al. 1998, Astron. Nachr., 319, 47
Ueda, Y. , et al. 1999a, ApJ, 518, 656
Ueda, Y., Inoue, H., Ogawara, Y., Fujimoto, R., Yamaoka, K., & Kii, T., Gotthelf, E. V. 1999b, ISAS Research Note, 688, 1.
Ueda, Y., et al. 2000, Adv. Space Res., 25, 839
Veron-Cetty, M. P. & Veron, P. 1998, ESO Sci. Rep., 18, 1